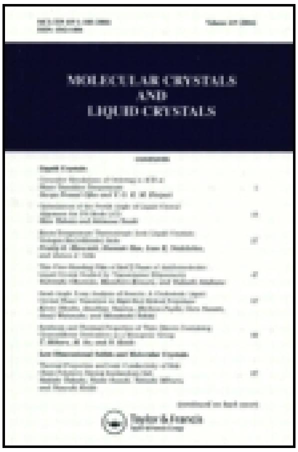

Molecular Crystals and Liquid Crystals Science and Technology. Section A. Molecular Crystals and Liquid Crystals

Publication details, including instructions for authors and subscription information:
http://www.tandfonline.com/loi/gmcl19

Study of Molecular Orientational States and Dielectric Properties of Surface Stabilized Ferroelectric Liquid Crystals

Nobuyuki Itoh [a] , Mitsuhiro Koden [a] , Shuji Miyoshi [a] & Tadashi Akahane [b]

[a] Functional Devices Laboratories, SHARP Corporation, 273-1 Kashiwa, Kashiwa, Chiba 277, Japan. Former Address: Central Research Laboratories, SHARP Corporation, 2613-1 Ichinomoto-cho, Tenri, Nara, 632, Japan

[b] Department of Electrical Engineering, Faculty of Engineering, Nagaoka University of Technology, Kamitomioka 1603-1, Nagaoka, Niigata, 940-21, Japan

Version of record first published: 23 Sep 2006.

To cite this article: Nobuyuki Itoh , Mitsuhiro Koden , Shuji Miyoshi & Tadashi Akahane (1995): Study of Molecular Orientational States and Dielectric Properties of Surface Stabilized Ferroelectric Liquid Crystals, Molecular Crystals and Liquid Crystals Science and Technology. Section A. Molecular Crystals and Liquid Crystals, 263:1, 333-375

To link to this article: http://dx.doi.org/10.1080/10587259508033597

Mol. Cryst. Liq. Cryst. 1995, Vol. 263, pp. 333–375
Reprints available directly from the publisher
Photocopying permitted by license only

Amsterdam B. V. Published under license by
Gordon and Breach Science Publishers SA
Printed in Malaysia

STUDY OF MOLECULAR ORIENTATIONAL STATES AND DIELECTRIC PROPERTIES OF SURFACE STABILIZED FERROELECTRIC LIQUID CRYSTALS

NOBUYUKI ITOH, MITSUHIRO KODEN, SHUJI MIYOSHI
and TADASHI AKAHANE †
Functional Devices Laboratories, SHARP Corporation,
273-1 Kashiwa, Kashiwa, Chiba 277, Japan
(Former Address;
Central Research Laboratories, SHARP Corporation,
2613-1 Ichinomoto-cho, Tenri, Nara 632, Japan)
† Department of Electrical Engineering, Faculty of Engineering,
Nagaoka University of Technology, Kamitomioka 1603-1, Nagaoka,
Niigata 940-21, Japan

Abstract The study of the molecular orientational states and the dielectric properties of surface stabilized ferroelectric liquid crystals (SSFLCs) was reviewed. The molecular orientational models were presented and they gave us a total understanding of the orientational states which appear in SSFLCs with parallel rubbing. Using the molecular orientational models, the dielectric properties of SSFLCs were studied. Three dielectric permittivities were measured for each of two samples, the permittivity of the homeotropic cell and the permittivity of the planar homogeneous cell with and without the DC bias, and then the dielectric tensor components were calculated based on the molecular orientational models. Results for Merck SCE-8 are reported. The novel frequency dependence of the dielectric biaxiality was found. The sign of the dielectric biaxiality inverted around 1kHz, being negative at low frequencies and positive at high frequencies. The relationship between the dielectric behavior of SSFLC cells and the dielectric biaxiality is discussed.

INTRODUCTION

The molecular orientational states and the dielectric properties of surface stabilized ferroelectric liquid crystals (SSFLCs)[1] were studied. They are responsible for the characteristics of SSFLC devices. First, the smectic layer structure of various SSFLCs were studied by using the high resolution X-ray. The relationship between the layer tilt angle of the chevron structure and the optical molecular tilt angle was confirmed. The molecular orientational states of SSFLCs were classified by the optical viewing conditions and the relationship between the directions of the chevron layer structure and surface pretilt. The molecular orientational models of the states were considered and illustrated with regard the experimental results. We obtained the useful informations from the optical simulations using the models. The effect of the surface pretilt angle on the orientational and optical properties of SSFLCs is discussed. The principal dielectric permittivities of SSFLCs were measured by the MOM (molecular orientational model) method. The theory and experimental procedure of the MOM method are explained. The novel dielectric behavior of SSFLC cells under the DC biasing field and the inversion of the sign of the dielectric biaxiality at the different frequencies were observed. The importance of the dielectric biaxiality on the dielectric behavior of SSFLC cells is discussed.

X-RAY STUDY ON SMECTIC LAYER STRUCTURE[2]

The discussion of the smectic layer structure is necessary before the molecular orientational study. The smectic layer structure of SSFLCs with parallel alignment but a few materials[3] is characterized by the chevron structure.[4,5] In the early days of this field, two important things were derived from a few FLC materials. The layer tilt angle was independent of the surface treatment, suggesting that the layer tilt angle was determined by the intrinsic properties of the ferroelectric liquid crystal (FLC) bulk.[4,5] The layer tilt angle was slightly smaller than the optical molecular tilt angle.[3,6] This discrepancy can be explained by recognizing the difference between the optical molecular tilt angle, resulting from the rigid central core, and the structural molecular tilt angle, overall the zigzag molecular structure[7,8] which includes the flexible alkyl chains.

We precisely investigated the layer structures of several SSFLCs with various FLC materials exhibiting different optical molecular tilt angles, and confirmed a correlation between the layer tilt angle of the chevron structure and the optical molecular tilt angle.

Experimental

The X-ray cells were made using micro cover glass plates about 150μm thick in order to avoid X-ray absorption. A high pretilt polyimide PSI-A-2001 (supplied by Chisso Co. Ltd.) and a low pretilt PVA were used in order to study the effect of the pretilt angle on the layer structure. The rubbing direction was parallel and the cell thickness was about 2μm. All measurements were performed at the room temperature (around 25℃). The pretilt angles were measured by the capacitance-magnetic field curves (C-H curves) method[9] using the antiparallel thick (about 50μm) cells for nematic liquid crystal E-8 (supplied by E.Merck). The pretilt angle θ_p of PSI-A-2001 was 15° and that of PVA was 0.5°. Six FLC materials in Table I which exhibited the different tilt angles were used. The tilt angles were measured observing the half of the two extinction positions of normal SSFLC cells having usual glasses with an ITO when a square wave voltage (± 10V/μm) was applied under cross nicol of an Olympus polarizing microscope. The X-ray scattering measurements were made using Rigaku RU-200B (50kV, 200mA).

TABLE I Physical properties of FLC materials used for X-ray study.

FLC material	Transition temperature/℃ $\mathrm{C} \cdot \mathrm{S_C}^{*} \cdot \mathrm{S_A} \cdot \mathrm{N} \cdot \mathrm{I}$	Apparent tilt angle/° (25℃)
mixture A[a]	·<RT· 55· 82· 93	17
CS-1014[b]	·<RT· 54· 69· 81	21
CS-1022[c]	·<RT· 60· 73· 85	25
ZLI-3654[d]	·<RT· 62· 76· 86	25
ZLI-3489[e]	·<RT· 65· 71· 87	29
FELIX-002[f]	·<RT· 70· 77· 87	33

b,c) supplied by Chisso. Co. Ltd.

d,e) supplied by E. Merck

f) supplied by Hoechst AG

Results and Discussion

The examples of the X-ray diffraction profiles are shown in Figure 1. Figure 1(a) shows mixture A with PSI-A-2001 and 1(b) shows FELIX-002 with PVA. In Figure 1, β is the angle between the incident X-ray and the smectic layer normal. The peaks of all profiles were sharp, and their positions and intensity were symmetric around the surface normal ($\beta = 90°$). The typical chevron layer structure was formed. Because of the chevron structure, measured optical tilt angles are the apparent tilt angles $\theta_{\text{app.}}$ which are slightly larger than the tilt angle θ, the half of the cone angle when an electric field is applied as shown in Figure 2. In Figure 2, **n** is the director, **p** is the spontaneous polarization vector, $\mathbf{n}_{xz}$ is the projection of **n** on the boundary XZ plane and z represents the perpendicular line of the cone. The electric field **E** is applied along the cell thickness direction Y. The relationship between the apparent tilt angle $\theta_{\text{app.}}$ and the tilt angle θ, is expressed as

$$\theta_{\text{app.}} = \tan^{-1}(\tan\theta \cdot \sec\delta) . \qquad (1)$$

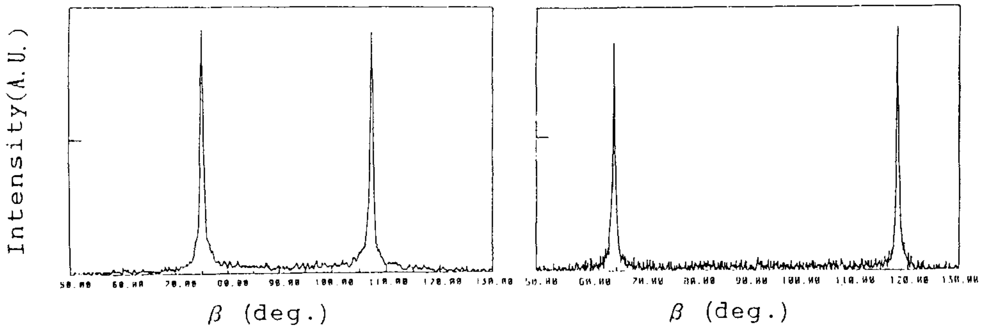

(a) (b)

FIGURE 1 X-ray scattering profiles:(a)mixture A with PSI-A-2001 and (b)FELIX-002 with PVA.

Figure 3 shows the relationship between the tilt angle θ and the layer tilt angle δ. The circles and crosses with the letters a)~f) in Figure 3 and Figure 4, represent the data of FLC materials shown in Table I by identical letters. The dashed lines indicate the approximation that the layer tilt angle is equal to the tilt angle. It is found that the layer tilt angle is slightly smaller than the optical tilt angle. Figure 4 shows the graph of the ratio κ ($= \delta / \theta$) versus θ. The variable $|\kappa|$ is around 0.9 and exhibits the tendency to gradually decrease as θ increases. This result is interpreted based on the hypothesis that the zigzag molecular structure of FLC, exhibiting a large tilt angle is more marked than that of FLC, exhibiting a small tilt angle. The difference between the aligning films were not recognized.

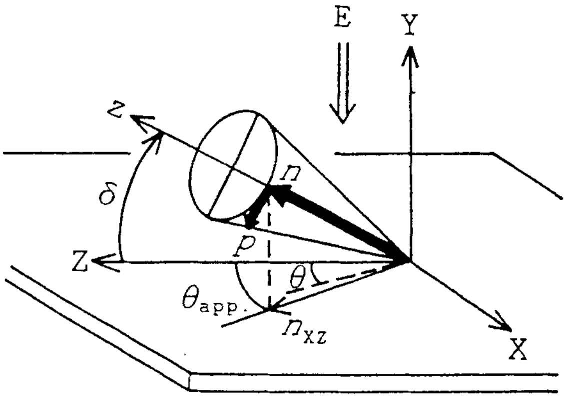

FIGURE 2 The coordinate system of the tilted layer structure. Here θ is the tilt angle and $\theta_{app.}$ is the apparent tilt angle.

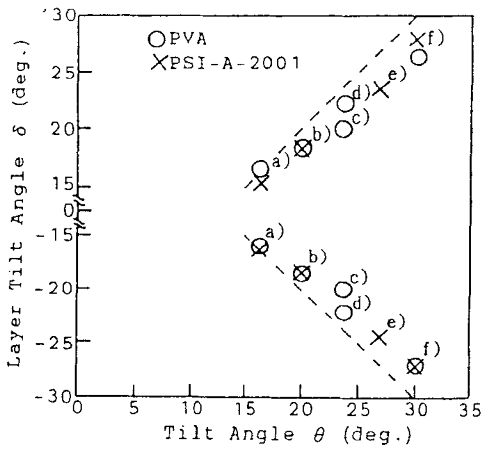

FIGURE 3 Relationship between the layer tilt angle and the tilt angle. See text for explanation.

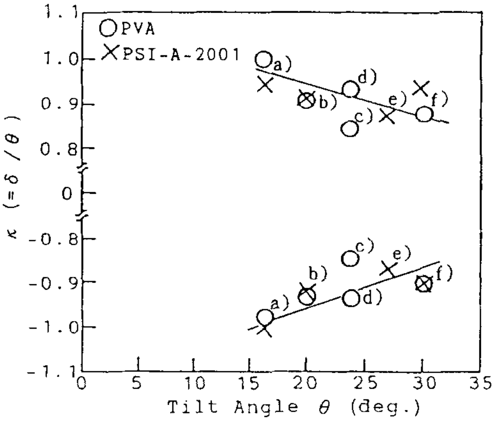

FIGURE 4 Correlation between the ratio of the layer tilt angle to the tilt angle, κ and the tilt angle. See text for explanation

STUDY OF MOLECULAR ORIENTATIONAL STATES[10]

The molecular orientational states of SSFLCs were analyzed by using a polarizing microspectroscope and optical calculations. And the models of molecular orientation were presented, summarizing the orientational states of SSFLCs with parallel rubbing. The X-ray study indicated that the chevron layer structure was determined by bulk properties of FLC, however, the molecular orientation in the smectic layer must be strongly influenced by the surface properties. The effect of the surface pretilt angle on the molecular orientation and optical properties of SSFLCs is discussed with regard to the simulation based on the molecular orientational models.

Two basic classifications of the molecular orientational states were reported. One classification is based on the optical viewing behavior when placed between crossed polarizers. The uniform (U) and twisted (T) states are defined by this classification.[11],[12] The uniform state shows extinction positions, but the twisted state shows only coloration positions without any extinction. Other classification is based on the relationship between the direction of the chevron layer structure and the direction of the surface pretilt. The C1 and C2 states are defined by this classification.[13] The C1 and C2 states are easily distinguished because the tilting direction of the chevron layer structure is confirmed by the direction of the zigzag defects,[14,15] and the direction of the surface pretilt is consistent with the rubbing direction.[16] Figures 5(a) and 5(b) show the C1 and C2 states related with the zigzag defect. Figure 5(c) shows the smectic layer models of the C1 and C2 states.

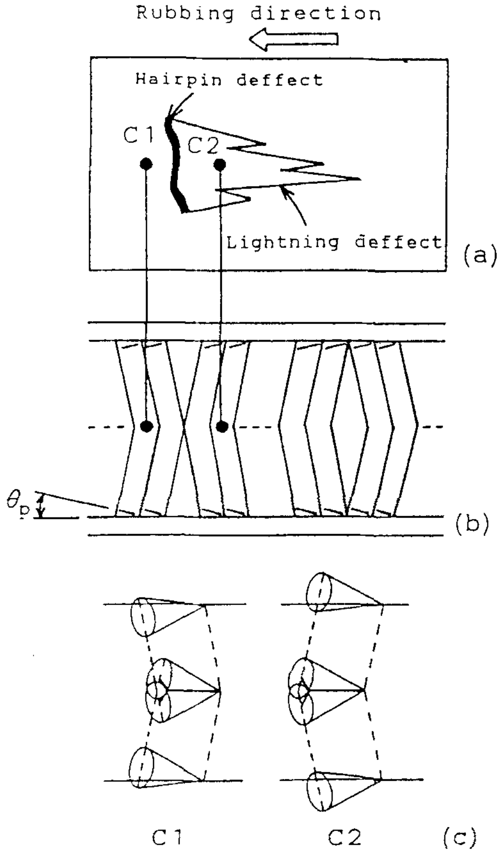

FIGURE 5 The C1 and C2 states, distinguished by the relationship between the direction of the chevron layer structure and the direction of the surface pretilt, as shown in (a) and (b). The tilting direction of the chevron layer structure is confirmed by the direction of the zigzag defects, as shown in (b). (c) The smectic layer models of the C1 and C2 states.

The four states, C1U (C1-uniform), C1T (C1-twisted), C2U (C2-uniform) and C2T (C2-twisted) were found in SSFLC cells by investigating a lot of samples aligned by various aligning films with parallel rubbing.[17] These four states are expressed by the combination of above two classifications.

Experimental

Three FLC materials exhibiting different tilt angles, and six polyimide aligning films exhibiting different pretilt angles, were used. The FLCs were CS-1014 supplied by Chisso Co., Ltd., SF-1212 blended at our laboratory, and SCE-8 supplied by E. Merck. The aligning films were PI-X, PSI-A-2101, PSI-A-X018, PI-Z, PSI-A-2001 and PSI-A-X021 supplied by Chisso Co., Ltd. The apparent tilt angle, the layer tilt angle and the pretilt angle were measured by using a polarizing microscope, the X-ray and the C-H curves, respectively, and are summarized in Table II and Table III. As it is known that the baking temperature of polyimide affects the pretilt angle,[18] the baking temperatures are also shown in Table III. The aligning films were formed on glass plates with an ITO electrode and an insulating film by spin coating, and were then baked and rubbed. Thin SSFLC cells (about 1.5μm) rubbed in a parallel direction were fabricated using silica balls as the spacer, and were filled with the FLC materials. The cells were mounted in a Mettlar FP82 hot stage and positioned between the cross nicol polarizers of an Olympus microscope. The memory angle θ_m was defined as the half angle between two extinction positions when no field was applied. An Orc polarizing microspectroscope TFM-120CFT was used to measure the transmitted light of small areas, such as the inside of the zigzag defect.

Results and Discussion

The different orientational states of SSFLCs with the different aligning films for the same FLC are shown. Figure 6 shows the polarized optical micrographs of the cell used with FLC CS-1014 and the high pretilt aligning film PSI-A-2001 ($\theta_p = 15°$). Figure 7 shows the micrographs of the cell used with CS-1014 and the low pretilt aligning film PI-X ($\theta_p = 3°$). Both micrographs were taken in the

TABLE II Tilt angles and layer tilt angles of FLC materials used for molecular orientational study at 25℃.

FLC material	Apparent tilt angle/°	Layer tilt angle/°	Tilt angle/°
CS-1014†	21.0	18.0	20.0
SF-1212‡	9.5	9.0	9.4
SCE-8§	22.0	19.5	21.0

† supplied by Chisso Co., Ltd.

‡ our blending mixture.

§ supplied by E. Merck.

TABLE III Baking temperatures and pretilt angles of aligning films used for molecular orientational study.

Aligning film†	Baking temperature/℃	Pretilt angle/°
PI-X	200	3
PSI-A-2101	200	6
PSI-A-X018	250	10
PI-Z	250	10
PSI-A-2001	200	15
PSI-A-X021	250	20

† All aligning films were supplied by Chisso Co., Ltd.

crossed nicol position at 25℃. The C1 and C2 states are identified on each side of the zigzag defects. The layer normal is parallel to the polarizer in Figure 6(a) and Figure 7(a). Figure 6(b) and Figure 7(b) show the viewing states when the cells are rotated from the positions of Figure 6(a) and Figure 7(a), respectively. Only the C2 state shows the extinction position (C2U) in Figure 6(b), and the C2 state showed only the C2U state everywhere in this PSI-A-2001's cell. Both the C1 and C2 states show the extinction position (C1U and C2U) in Figure 7(b). Figure 6(c) shows the viewing state when the cell is rotated further from the position of Figure 6(b). Only the C1 state showed the extinction position (C1U) at this position, and the small C1 state without any extinction position (C1T) were seen. Figure 7(c) shows

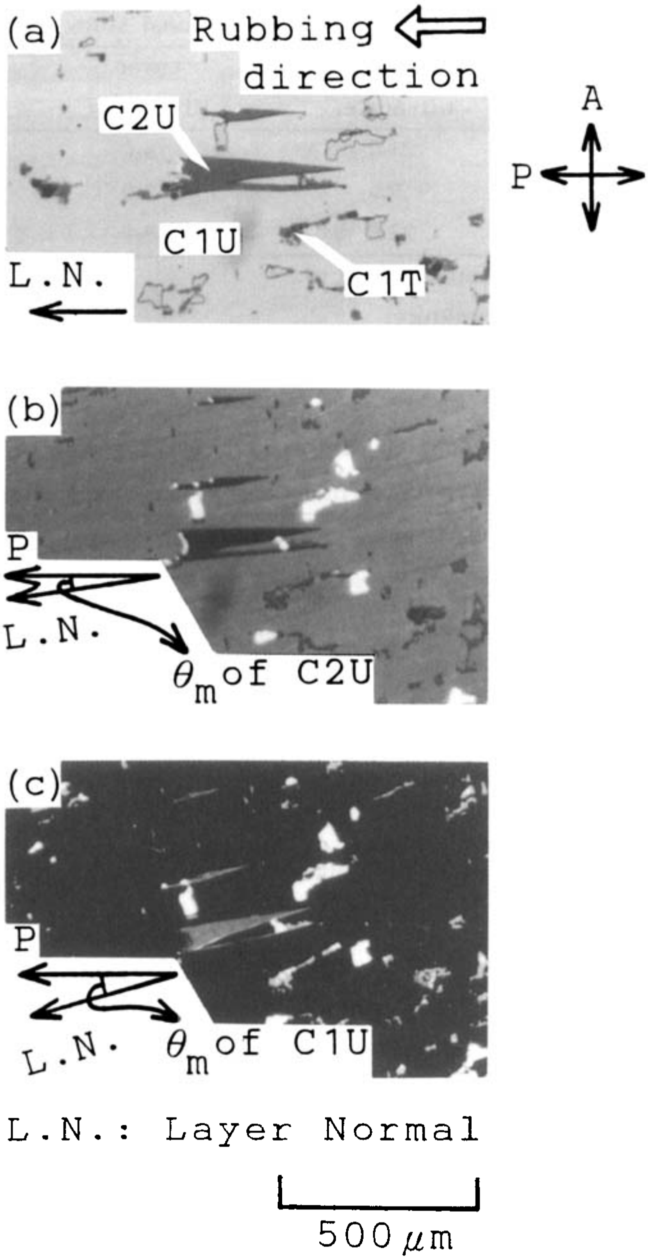

FIGURE 6 The polarized optical micrographs of the sample used with CS-1014 and high pretilt aligning film PSI-A-2001. See text for explanation. L.N. denotes the layer normal.
See Color Plate XI.

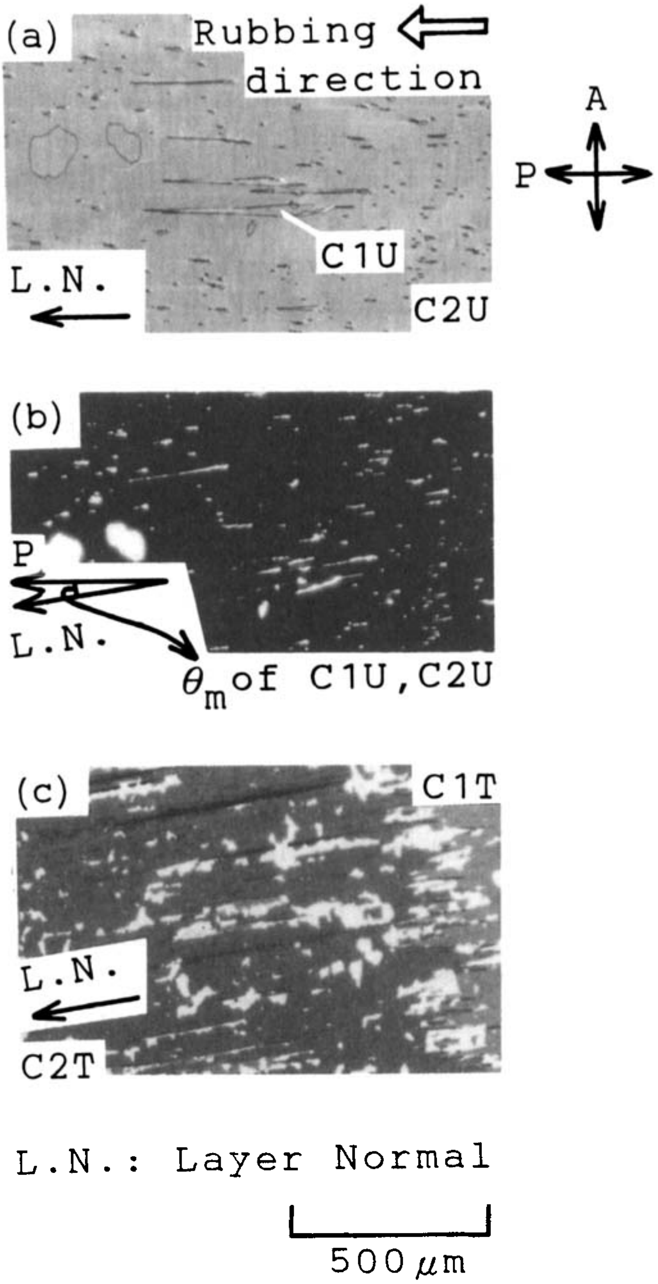

FIGURE 7 The polarized optical micrographs of the sample used with CS-1014 and low pretilt aligning film PI-X. See text for explanation. L.N. denotes the layer normal.
See Color Plate XII.

another area of the cell. Both the C1 and C2 states showed only coloration positions without any extinction positions (C1T and C2T) in this area. From Figure 6 and Figure 7, it is found that the four states, C1U, C1T, C2U and C2T can appear in SSFLCs with parallel rubbing, and that SSFLCs with high pretilt aligning films show only one state with extinction positions in the C2 state. This type of the C2 state is defined as a special case of the C2U state, called the high pretilt C2U state. On the other hand, both the C1U and C1T states can appear regardless of the pretilt angle. The C1U and C2U states are interesting from the practical point of view because they have possibility to achieve a high contrast.

The memory angles of the C1U and C2U states are shown schematically in Figure 6 and Figure 7. The memory angle of the C1U state is greater than that of the C2U state in the high pretilt cell [Figures 6(b) and 6(c)]. However, the difference between the memory angles of the C1U and C2U states is very small in the low pretilt cell [Figure 7(b)]. It is expected that the memory angle depends on the surface pretilt angle. The temperature dependences of the memory angles of the C1U and C2U states were measured for all cells, and are shown in Figure 8. The solid lines represent the apparent tilt angle behavior. There is little difference in the apparent tilt angles among the cells, indicating the reliability of the cells. Some cells used with FLC SF-1212, and aligning films except PI-X and PSI-A-2101, showed only the C1 state with slight zigzag defects. According to Kanbe et al.,[13] it is difficult for the C2 state to appear if the tilt angle is small or the surface pretilt angle is high. The memory angle of the C2U state was almost independent of the aligning films. The memory angle of the C1U state of CS-1014 and SCE-8 strongly depended on the aligning films. The aligning film dependence of the memory angle of SF-1212 was not strong.

The optical properties of SSFLC cell used with CS-1014 and PSI-A-2001, were measured in order to analyze the molecular orientations. The wavelength dependences of the memory angles of the C1U and C2U states are shown in Figure 9. The C1U and C2U states exhibit the opposite wavelength dispersion with respect to each other. The transmission spectra of both memory states, the bright and dark

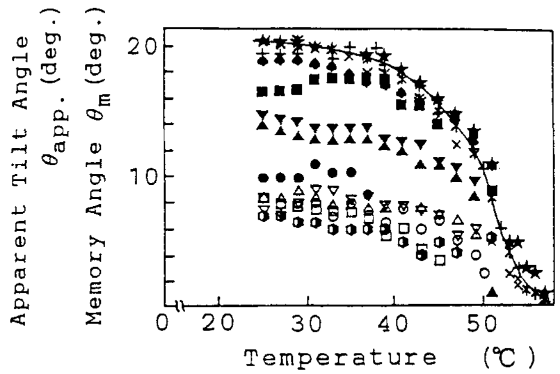

(a) CS-1014

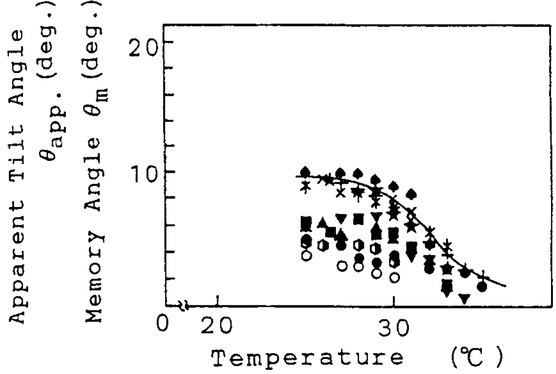

(b) SF-1212

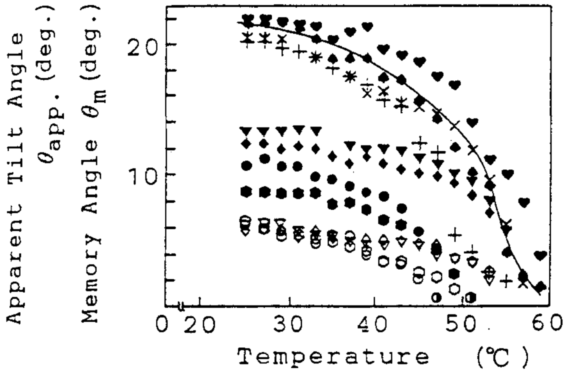

(c) SCE-8

FIGURE 8 The temperature dependence of the apparent tilt angle (♠,+,×,♥,∗,★), the memory angle of the C1U state (⬢,●,▲,◆,▼,■) and the memory angle of the C2U state (⬡,○,△,◇,▽,□) with various aligning films (PI-(♠,⬢,⬡), PSI-A-2101(+,●,○), PSI-A-X018(×,▲,△), PI-Z(♥,◆,◇), PSI-A-2001(∗,▼,▽) and PSI-A-X021(★,■,□)) for (a) CS-1014, (b) SF-1212 and (c) SCE-8. The lines are the apparent tilt angle behavior.

states, prepared by applying a pulsed electric field, are shown in Figure 10. The transmission spectra indicate that a high contrast ratio is obtained not by the C2U state, but by the C1U state. The large memory angle contributed to a high contrast ratio. The transmitted light was calculated theoretically in order to discuss these optical properties.

The molecular orientational models of the C1U, C1T, C2U, C2T and the high pretilt C2U states are shown in Figure 11. The molecules are almost uniformly tilted at one side from the layer normal in the C1U and C2U models. The C1T and C2T models are the half splayed states.[19,20] The boundary surfaces in the C2 state do not have wide regions wherein the molecules can exist stably, as shown in Figure 5(c). The c-directors at the surfaces are almost perpendicular to the substrate in the high pretilt C2U model. The molecules at surfaces can move easily even in the C2 state if the pretilt is low. These states are assumed to switch between two elastically equivalent states for the stable memory effect.

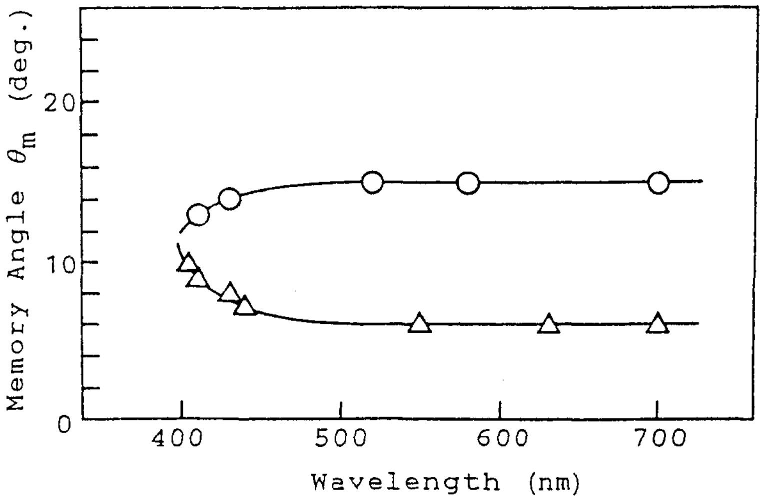

FIGURE 9 The wavelength dependences of the memory angle of the C1U state(○) and the C2U state(△).

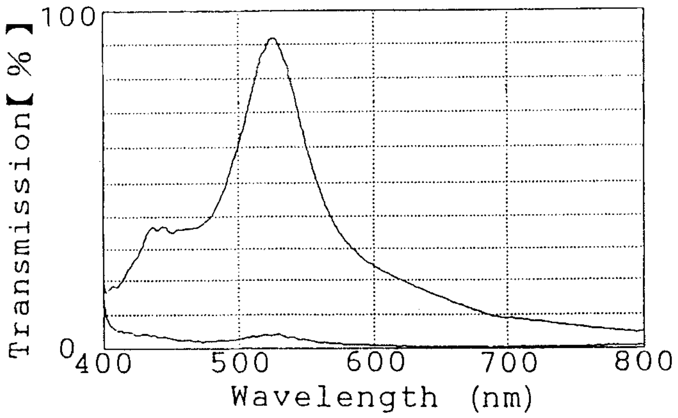

(a)C1U

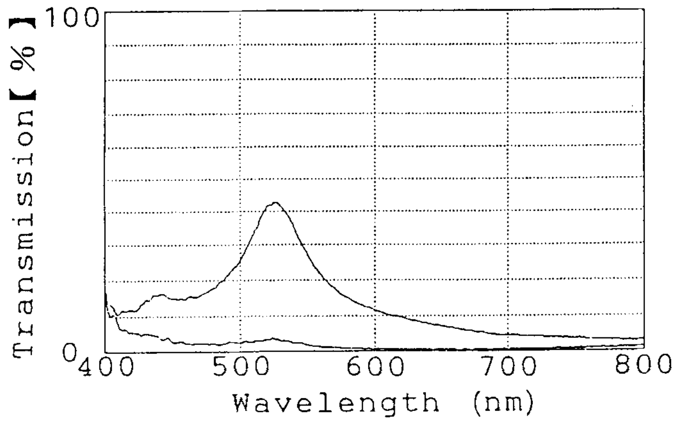

(b)C2U

FIGURE 10 The transmission spectra of the (a) C1U and (b) C2U memory states. The upper curves represent the bright spectra and the bottom curves represent the dark spectra.

Figure 12 shows the coordinate systems. In Figure 12, **n** is the director, **c** is the **c**-director and **p** is the spontaneous polarization vector. It is assumed that the tilt angle θ and the layer tilt angle δ are constant, and the azimuthal angle Φ depends only on the cell thickness direction Y. The director is expressed as follows;

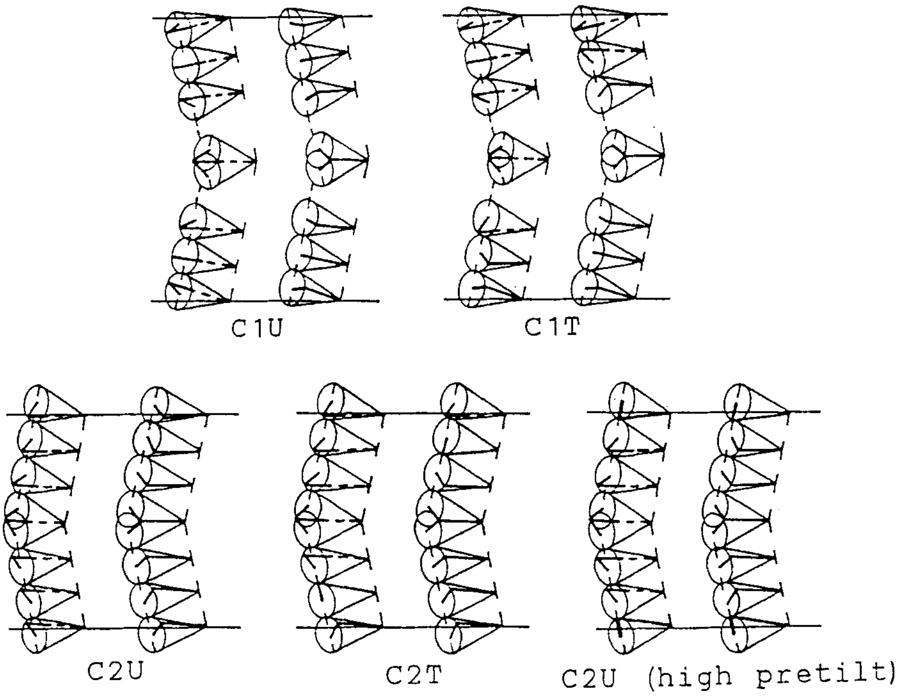

FIGURE 11 The molecular orientational models of SSFLCs, with a chevron layer structure.

$$\mathbf{n}\,(x,y,z)=(\sin\theta\cos\Phi\,,\ \sin\theta\sin\Phi\,,\ \cos\theta\ )\ , \tag{2}$$

and

$$\mathbf{n}\,(X,Y,Z)=\begin{pmatrix}\sin\theta\cos\Phi\\ \sin\theta\sin\Phi\cos\delta-\cos\theta\sin\delta\\ \sin\theta\sin\Phi\sin\delta+\cos\theta\cos\delta\end{pmatrix}. \tag{3}$$

The transmitted light was calculated by the Berreman 4 × 4 matrix method.[21] The dielectric tensor is determined by the director tilt angle γ and the director twist angle ϕ which are expressed as

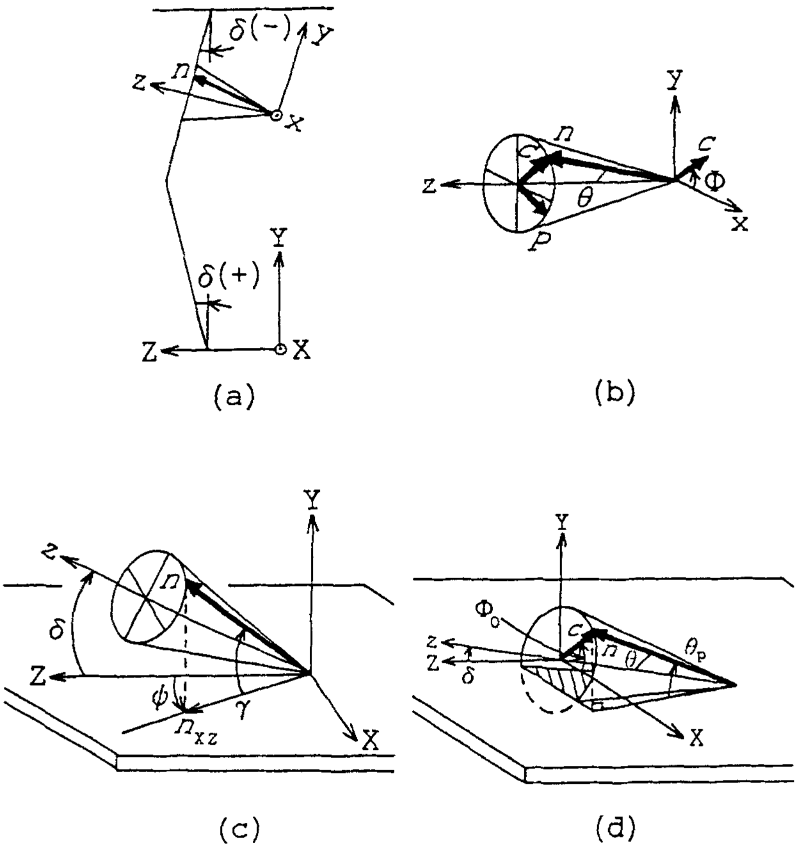

FIGURE 12 The coordinate systems used for calculations. Y and Z represent the cell thickness direction and the smectic layer normal, respectively, and z is the perpendicular line of cone. (a) The chevron layer system. (b) The cone system. (c) The director tilt angle γ and the director twist angle ϕ. (d) The scheme of the director at the surface.

$$\gamma = \sin^{-1}(\sin\theta \sin\Phi \cos\delta - \cos\theta \sin\delta) , \tag{4}$$

$$\phi = \tan^{-1}\left(\frac{\sin\theta \cos\Phi}{\sin\theta \sin\Phi \sin\delta + \cos\theta \cos\delta}\right) . \tag{5}$$

The pretilt angle θ_p is simply defined as Figure 12(d). The c-director pretilt Φ_0 is expressed by Eq. (6).

$$\Phi_0 = \sin^{-1}\left(\frac{\tan\delta}{\tan\theta} + \frac{\sin\theta_p}{\sin\theta\cos\delta}\right) . \quad (6)$$

It is assumed that Φ_0 at the bottom surface is $\pi/2$ and Φ_0 at the top surface is $-\pi/2$ for the high pretilt C2U. The azimuthal angle at the chevron interface Φ_{IN} is expressed as

$$\Phi_{IN} = \sin^{-1}(\tan\delta/\tan\theta) . \quad (7)$$

For simplicity, it is assumed that Φ changes with Y at a constant rate, ignoring the effect of the polarization electric field on the elastic deformation.[22] After Kawaida et al.,[23] the wavelength dispersion of the refractive indices was taken into account. The wavelength dependences of the memory angles and the transmission spectra were calculated for CS-1014($\theta = 20.0°$, $\delta = 18.0°$) and PSI-A-2001($\theta_p = 15°$).

The calculated wavelength dependences of the memory angles are shown in Figure 13. Both the C1U and C2U models exhibit the same dispersion as the experimental results. Figure 14 shows the calculated transmission spectra. Both the C1U and C2U models show slight transmission in short wavelength regions of the dark states, and show a peak around 500nm of the bright states. The calculated results were almost consistent with the experimental results, indicating the approximate validity of our orientational models. The dependences of the memory angles on the surface pretilt angle were simulated using the models, and are shown in Figure 15 with the experimental results of Figure 8 at 25℃. In every case, the calculated memory angle is the value for wide visible wavelengths. For every material, good agreement between the simulated and the experimental results was confirmed.

The director profiles were calculated in order to discuss above results. All calculations were performed for CS-1014. In Figure 16, the director twist angle ϕ is shown as a function of the cell thickness direction Y for various surface pretilt angles, where ϕ_{IN} represents the director twist angle at the chevron interface and is expressed as

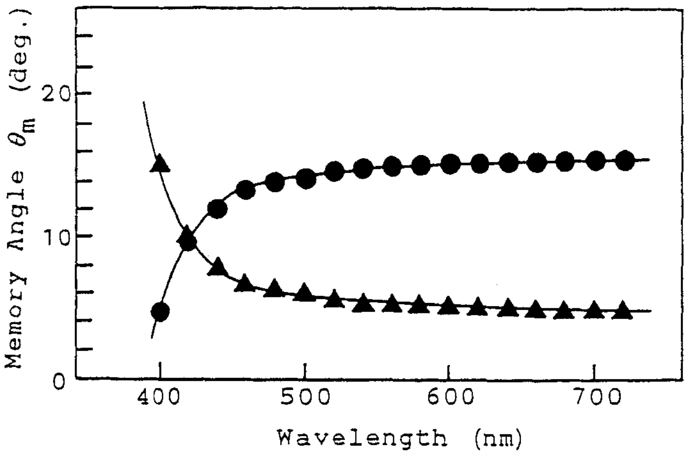

FIGURE 13 The calculated wavelength dependences of the memory angle of the C1U state(●) and the C2U state(▲).

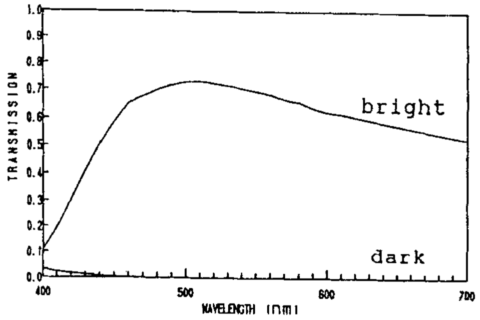

(a) C1U

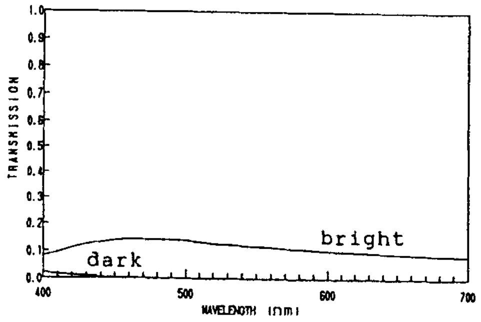

(b) C2U

FIGURE 14 The calculated transmission spectra, of the (a) C1U and (b) C2U state.

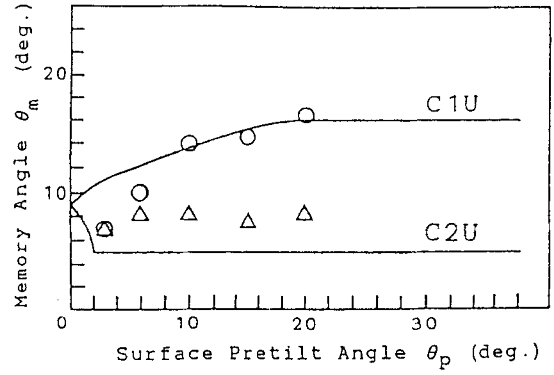

(a) CS-1014

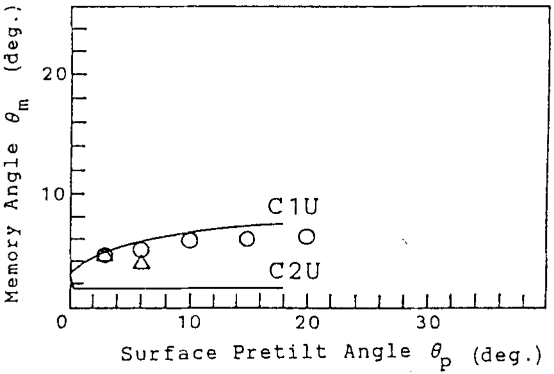

(b) SF-1212

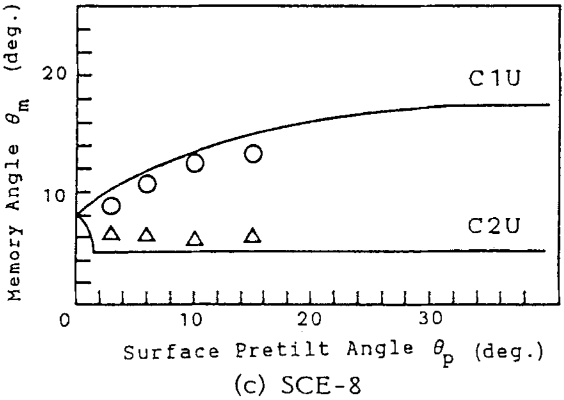

(c) SCE-8

FIGURE 15 The relationships between the surface pretilt angle and the memory angle of the C1U state(○), and the of the C2U state(△) for (a) CS-1014, (b) SF-1212 and (c) SCE-8. The lines are the simulated results.

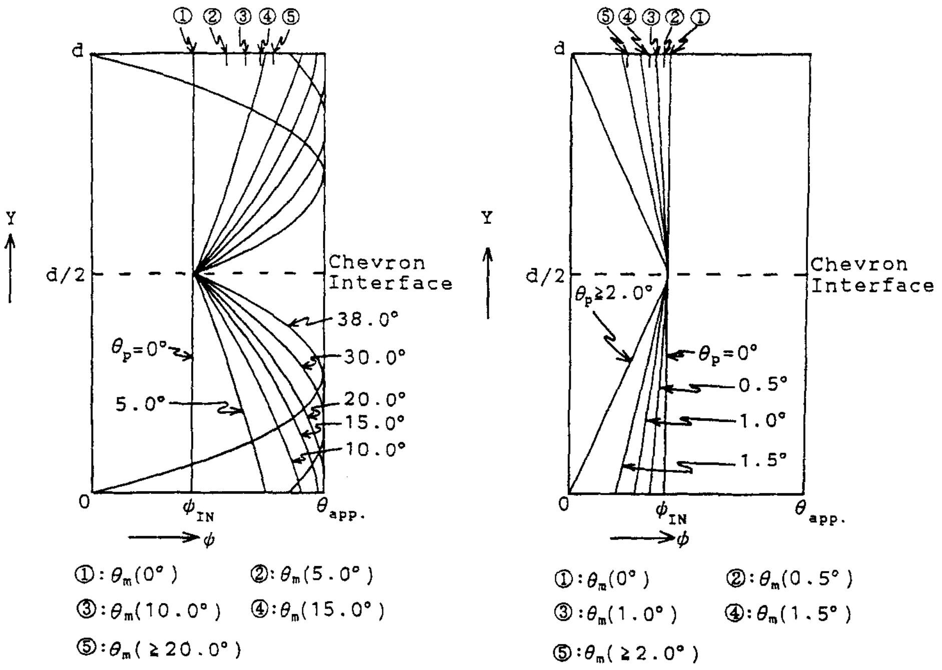

(a) C1U (b) C2U

FIGURE 16 The calculated director profiles and the memory angles for various surface pretilt angles for the (a) C1U and (b) C2U states. The memory angles are denoted by encircled numerals.
In (a), 1: θ_m ($\theta_p = 0°$), 2: θ_m ($\theta_p = 5.0°$), 3: θ_m ($\theta_p = 10.0°$), 4: θ_m ($\theta_p = 15.0°$) and 5: θ_m ($\theta_p \geq 20.0°$).
In (b), 1: θ_m ($\theta_p = 0°$), 2: θ_m ($\theta_p = 0.5°$), 3: θ_m ($\theta_p = 1.0°$), 4: θ_m ($\theta_p = 1.5°$) and 5: θ_m ($\theta_p \geq 2.0°$).

$$\phi_{IN} = \cos^{-1}(\cos\theta / \cos\delta)\ . \qquad (8)$$

The memory angles of each case are indicated simultaneously in Figure 16. In Figure 17, the calculated transmission spectrum for each case is shown. These figures indicate that the memory angle and the transmission of the bright state depend on the surface pretilt angle. It is found that the memory angle θ_m is determined by the following equation,

$$\theta_{\mathrm{M}} \doteqdot (\phi_0 + \phi_{\mathrm{IN}})/2 \, , \tag{9}$$

where ϕ_0 is the director twist angle at the surface. The memory angle of the C1U state becomes large by increasing the surface pretilt angle and will be saturated at values of $\theta_{\mathrm{Msat.}}$ expressed as Eq. (10),

$$\theta_{\mathrm{Msat.}} \doteqdot (\phi_{\mathrm{IN}} + \theta_{\mathrm{app.}})/2 \, . \tag{10}$$

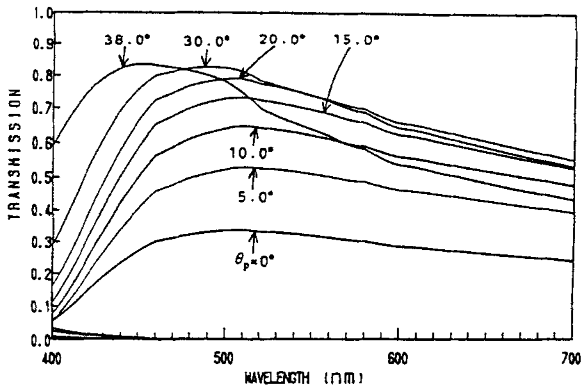

(a) C1U

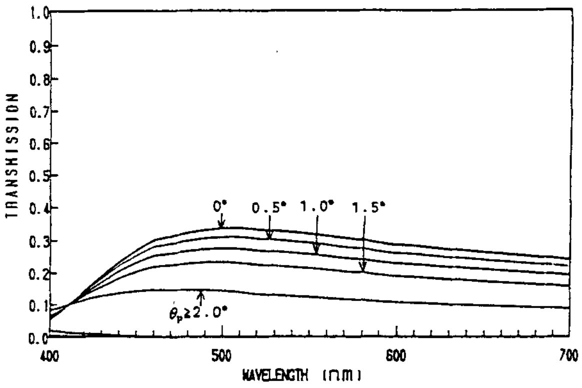

(b) C2U

FIGURE 17 The calculated transmission spectra for various surface pretilt angles of the (a) C1U and (b) C2U states.

On the other hand, the memory angle of the C2U state becomes large by decreasing the surface pretilt angle. The results in Figure 15 are well explained by the orientational models. However, the memory angle of the C2U state seems to be virtually constant because its surface pretilt dependence is very slight.

The orientational states which appear in SSFLC cells with parallel rubbing are summarized in Figure 18, expressed by the c-director orientations and director profiles.

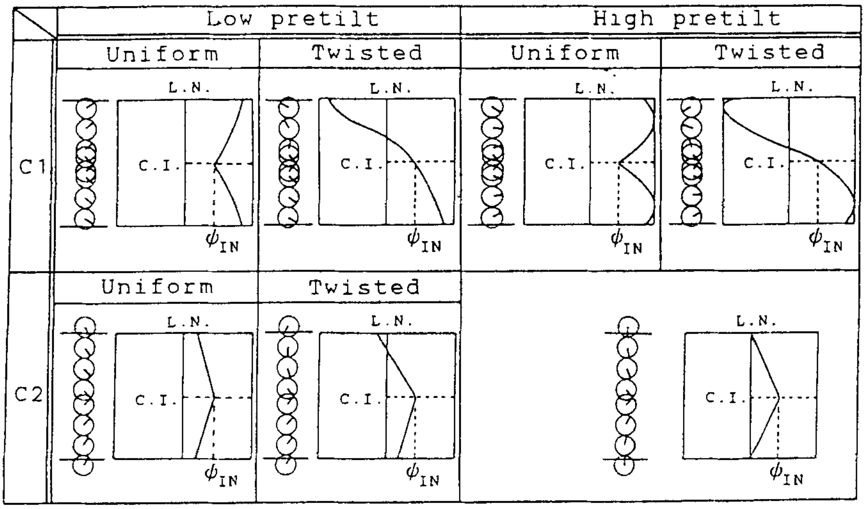

FIGURE 18 A summary of the orientational states in SSFLCs with the chevron layer structure.

DIELECTRIC PERMITTIVITY STUDY[24,25]

SSFLC devices using the $\tau - V_{MIN}$ mode have been reported[26,27] and this showed a fast line address time and a high contrast ratio.[28] In principle, the characteristics of the $\tau - V_{MIN}$ mode are dominated by the dielectric biaxiality and the spontaneous polarization.[29,30] The study of the dielectric permittivity is also important for SSFLC devices as well as the molecular orientational states. The measurement method which is based on the molecular orientational model is required in order to measure the principal dielectric permittivities of SSFLCs because of the complicated molecular orientational states. The theory and experimental procedure of the MOM (molecular orientational model) method are explained considering the effect of the structural deformation of the smectic layer. We measured the frequency dependence of the dielectric permittivities of SSFLCs, and found a novel behavior for the dielectric biaxiality. At last the importance of the dielectric biaxiality on the dielectric behavior of SSFLC cells is discussed.

Measurement Method of Principal Dielectric Permittivities

Three principal dielectric permittivity tensor of the biaxial FLC are defined as Figure 19. The permittivity in the tilt plane made by the symmetry axis of the smectic cone **z** and the director **n**, perpendicular to the long molecular axis is denoted as ε_1. The permittivity in the direction perpendicular to the long molecular axis and to the tilt plane, in the direction of the spontaneous polarization is denoted as ε_2. The permittivity in the direction of the long molecular axis is denoted as ε_3. Two dielectric anisotropies are defined as

$$\Delta\varepsilon = \varepsilon_3 - \varepsilon_1 , \tag{11}$$

$$\partial\varepsilon = \varepsilon_2 - \varepsilon_1 , \tag{12}$$

where $\partial\varepsilon$ is the dielectric biaxiality. The local dielectric permittivity tensor is

$$\bar{\varepsilon}(1,2,3) = \begin{pmatrix} \varepsilon_1 & 0 & 0 \\ 0 & \varepsilon_2 & 0 \\ 0 & 0 & \varepsilon_3 \end{pmatrix} . \tag{13}$$

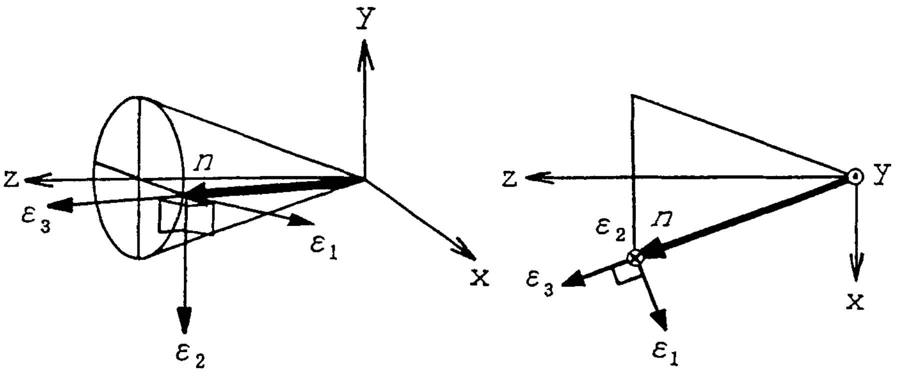

FIGURE 19 The definition of the principal dielectric permittivities of FLC.

The MOM method requires two differently aligned cells and uses three geometric systems which are illustrated in Figure 20. Though the apparent tilt angle $\theta_{\mathrm{app.}}$ was defined as the fully switched extinction angle, it is difined as the extinction angle under arbitrary voltage for the dielectric permittivity measurement. The first system is the homeotropic geometry [Figure 20(a)] and the measured dielectric permittivity is

$$\begin{aligned}\varepsilon_h &= \varepsilon_1 \sin^2\theta + \varepsilon_3\cos^2\theta \\ &= \varepsilon_1 + \Delta\varepsilon\cos^2\theta \ . \end{aligned} \qquad (14)$$

The second system is the planar homogeneous geometry with the chevron layer structure [Figure 20(b)] and the measured dielectric permittivity is

$$\begin{aligned}\frac{1}{\varepsilon_p} &= \frac{1}{d}\left(\int_0^{d/2}\frac{1}{\varepsilon_{YY}}\,dY + \int_{d/2}^{d}\frac{1}{\varepsilon_{YY}}\,dY\right) \\ &= \frac{1}{2(\Phi_{IN}-\Phi_0)}\int_{\Phi_0}^{\Phi_{IN}}\frac{1}{\varepsilon_{YY}}\,d\Phi + \frac{1}{2(\Phi_d-\Phi_{IN})}\int_{\Phi_{IN}}^{\Phi_d}\frac{1}{\varepsilon_{YY}}\,d\Phi \ . \end{aligned} \qquad (15)$$

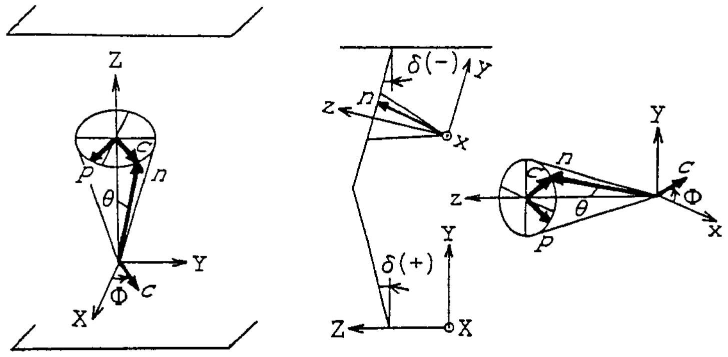

(a) homeotropic cell (b) planar homogeneous cell

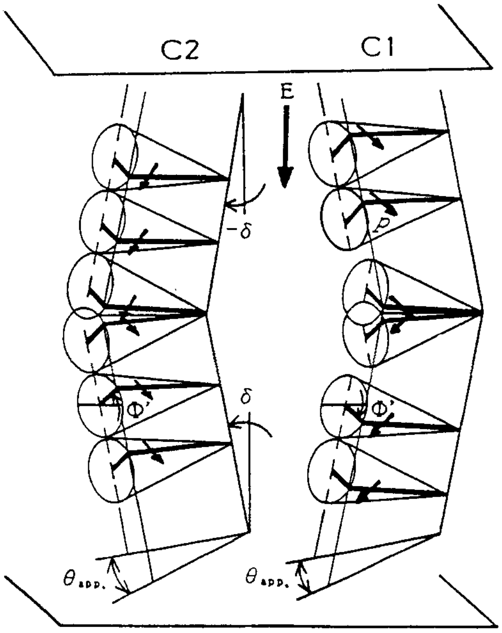

(c) homogeneous cell under DC bias

FIGURE 20 The geometries of the dielectric permittivity measurement.

Where ε_{YY} is the component of the permittivity tensor in the direction of the electric field and expressed as

$$\varepsilon_{YY} = \varepsilon_1 + \Delta\varepsilon\,[\sin\theta\cos\delta\sin\Phi(Y) - \cos\theta\sin\delta\,]^2 + \partial\varepsilon\cos^2\delta\cos^2\Phi(Y)\ . \qquad (16)$$

The azimuthal angle Φ is the function of the cell normal Y, d is the cell thickness and Φ_d is the **c**-director pretilt at the top surface. The last system is the planar homogeneous chevron geometry with a constant azimuthal angle Φ' under the DC bias [Figure 20(c)] and the measured dielectric permittivity is

$$\varepsilon_p' = \varepsilon_1 + \Delta\varepsilon\,(\sin\theta\sin\Phi'\cos\delta - \cos\theta\sin\delta\,)^2 + \partial\varepsilon\cos^2\Phi'\cos^2\delta\ . \qquad (17)$$

The three principal dielectric permittivities, ε_1, ε_2 and ε_3 are calculated from three experimental measured values of the equations (14), (15) and (17) by a coordinate transformation using the molecular orientational models of Figure 11. In particular the defect-free homogeneous molecular orientational states are required in order to solve equations (15) and (16) for the planar homogeneous cell.

Experimental

The dielectric permittivities of SCE-8 were measured. The homeotropic cell was made using the polyimide JALS-204 (Japan Synthetic Rubber Co., Ltd.), the cell thickness was 6μm. Two kinds of planar homogeneous cells rubbed in parallel directions were made using the polyimide PI-A and PSI-A-2001, respectively, the cell thickness was 1.5μm. The pretilt angle of PI-A was 5°. The dielectric permittivities were determined from capacitance measurements using a Hewlett Packard precision LCR meter (HP4284A). The polarized micrographs of the planar homogeneous cells are shown in Figure 21. The cell using PI-A (cell A) showed a stable defect-free homogeneous C2U state [Figure 21(a)], and the cell using PSI-A-2001 (cell B) showed a defect-free homogeneous C1U state by slow cooling down (∼1℃/min) from the isotropic phase under a square wave electric field (± 3.3V/μm, 1kHz) [Figure 21(b)]. The molecular orientation of the defect-free homogeneous states were distinguished by the memory angle. The memory angle of the cell A was 6.5° and that of the cell B was 13° The molecular orientational model for cell A is therefore the high pretilt C2U state because the surface pretilt angle is larger than the difference between the tilt angle and the layer tilt angle.

Figure 22 shows the behavior of the dielectric permittivity of the homeotropic cell. Figure 22(a) shows the temperature dependences at the different frequencies and Figure 22(b) shows the frequency dependence at 25℃. The dielectric permittivity of the homeotropic cell showed a frequency dispersion in the SmC* phase and a different temperature dependence at the different frequencies.

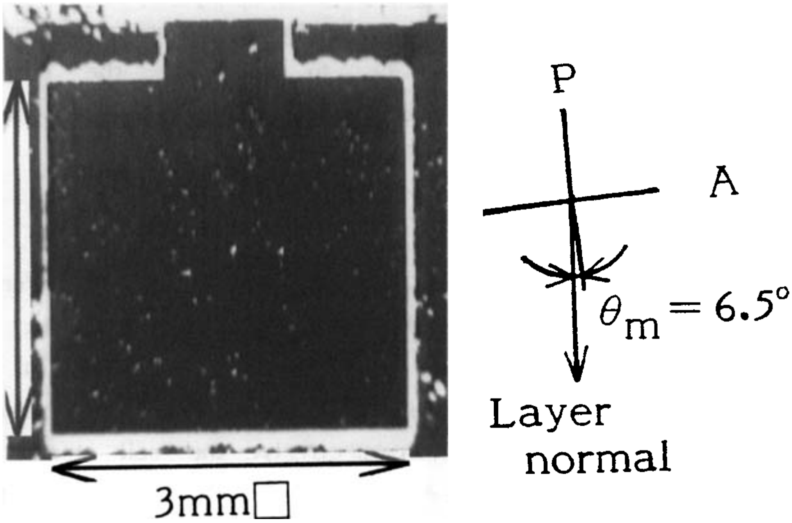

(a) cell A (C2U)

FIGURE 21 The polarized optical micrographs of the planar homogeneous cells. (a) cell A and (b) cell B.

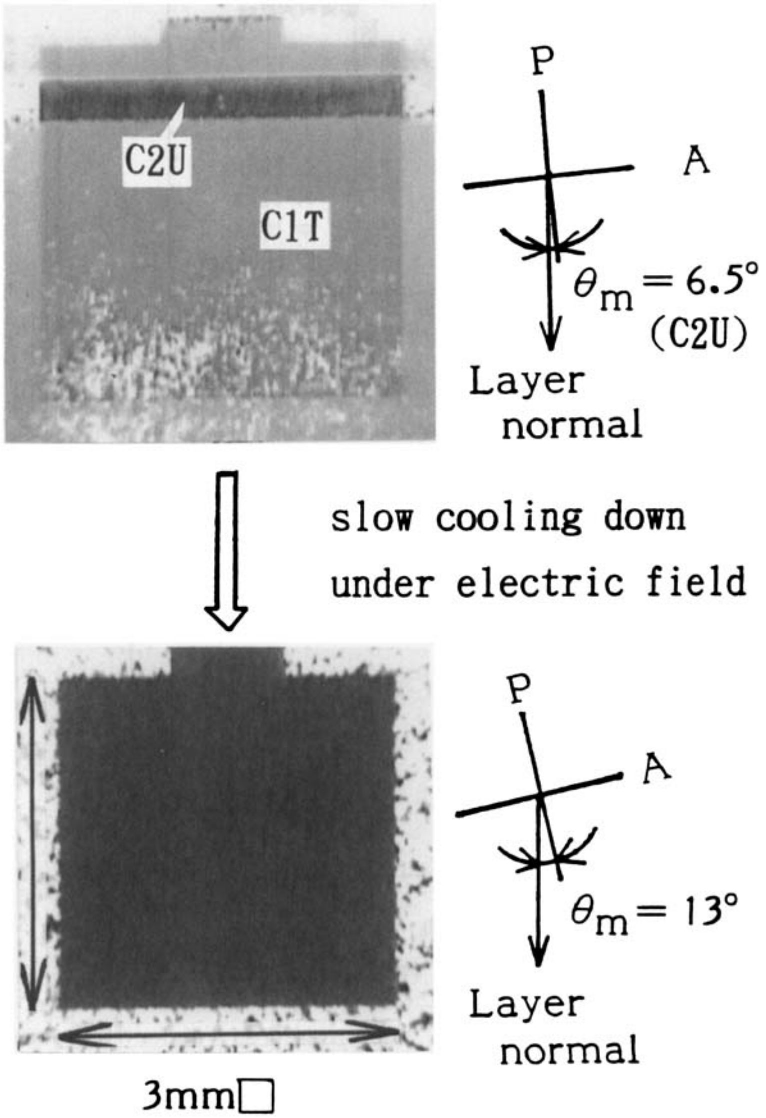

(b) cell B (C1U)

FIGURE 21 The polarized optical micrographs of the planar homogeneous cells. (a) cell A and (b) cell B. See Color Plate XIII.

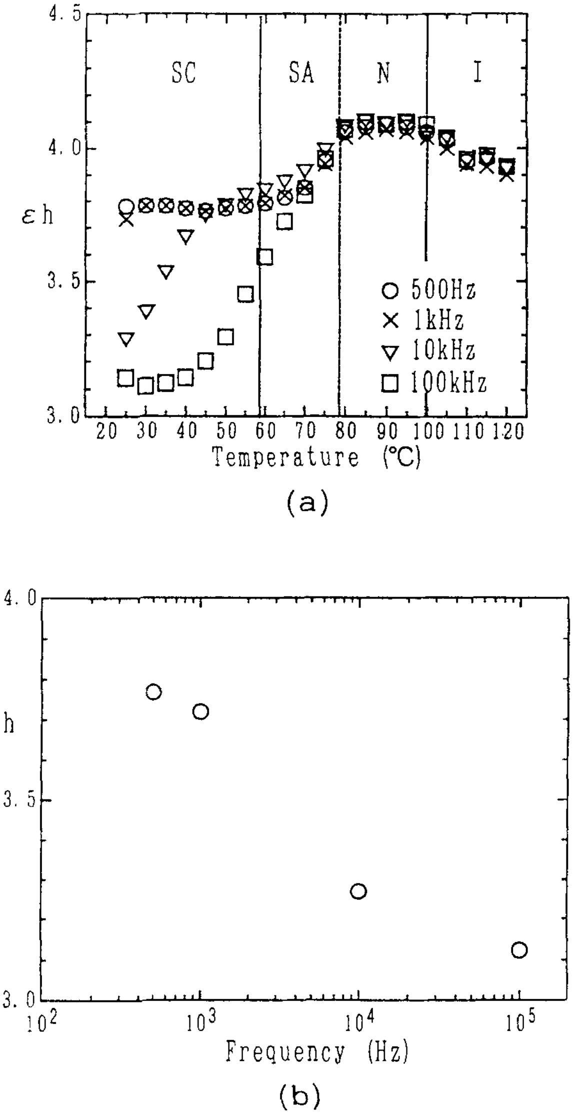

FIGURE 22 The behavior of the measured dielectric permittivity of the homeotropic cell. (a) The temperature dependences at different frequencies. (b) The frequency dependence at 25℃.

The dielectric permittivities of the planar homogeneous cells were measured with a 100mV$_{rms}$ capacitance probe voltage at 25℃. The spontaneous polarization is required to be rotated by the bias field not the capacitance probe voltage. The dielectric permittivities during biasing and after biasing, when the bias field is turned off, were measured as the bias voltage was increased. Figure 23 and Figure 24 show the voltage dependence of the dielectric permittivities during biasing and after biasing, respectively. Both the dielectric permittivities during biasing and after biasing showed a different bias voltage dependence at different frequencies. The dielectric permittivity during biasing shown in Figure 23 increased at 10kHz and 100kHz with increasing bias voltage, on the other hand it decreased at 500Hz. At 1kHz, the cell A did not show a large change in permittivity and cell B showed only slight decrease. Though the magnitudes of the dielectric permittivity of the two cells were different, the bias voltage dependences of the dielectric permittivity showed similar properties. The dielectric permittivity after biasing, shown in Figure 24, changed showing a threshold with increasing voltage. The dielectric permittivity after biasing also increased at 10kHz and 100kHz, decreased at 500Hz and did not show a large change at 1kHz, all for increasing bias voltage. The dielectric permittivity after biasing began to change above 10V.

Influence of Deformation of Smectic Layer Structure[31]

Figure 25 shows the polarized micrographs of the cell A before and after biasing; (a) before biasing (homogeneous C2U state), (b) after 8V biasing (similar to the initial state), (c) after 10V biasing (slight rooftop lines, pointed out by an arrow, appeared), (d) after 16V biasing (many rooftop lines appeared), (e) after 24V basing (slight stripes parallel to the smectic layer normal, pointed out by an arrow, appeared) and (f) after 30V biasing (many stripes appeared). These sequential texture change indicates the smectic layer structure changed from the chevron to the quasi-bookshelf.[32] The illustrated textures of these photographs are shown as insets in Figure 26. Figure 26 shows the dielectric permittivity of cell A at 10kHz, in Figure 24(a), and the observed texture. The rooftop lines are not illustrated in Figure 26(e) for clarity of the stripe pattern. The dielectric permittivity after the biasing began to change when the texture changed from the initial state to the rooftop texture and increased with increasing density of rooftop lines, beginning to saturate when the striped texture appeared. It is found that the dielectric permittivity of SSFLCs is strongly affected by the smectic layer deformation. The properties of the dielectric permittivity after biasing in Figure 24 give us the information about the smectic layer deformation.

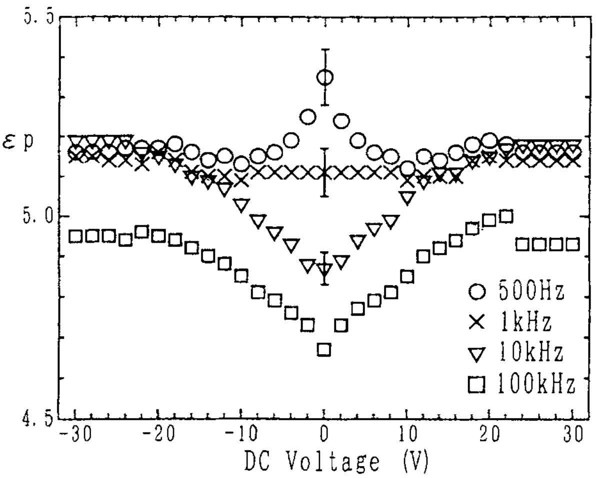

(a) cell A

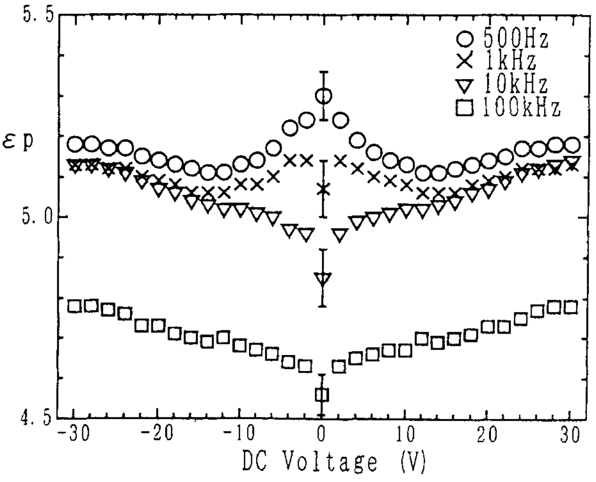

(b) cell B

FIGURE 23 The voltage dependences of the measured dielectric permittivities of the planar homogeneous cells during biasing. (a) cell A and (b) cell B.

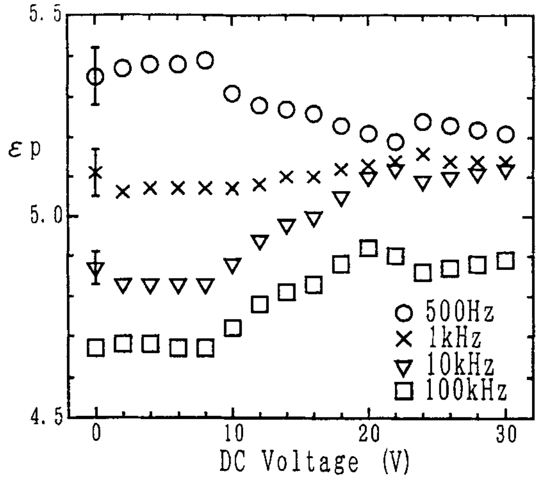

(a) cell A

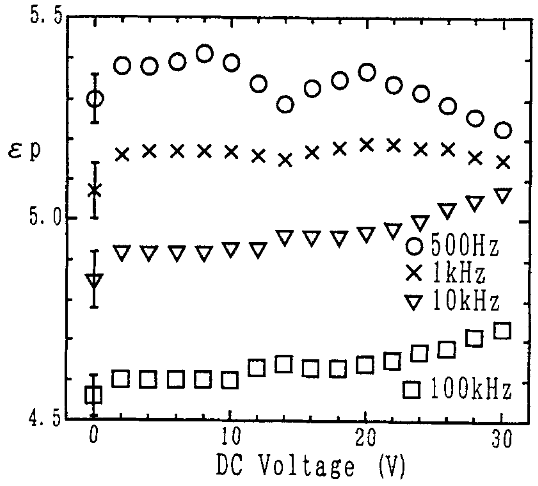

(b) cell B

FIGURE 24 The voltage dependences of the measured dielectric permittivities of the planar homogeneous cells after the biasing field is turned off. (a) cell A and (b) cell B.

The MOM measurement must be performed under the condition of no smectic layer deformation. The appropriate bias voltage can be determined by checking the dielectric permittivity after the biasing

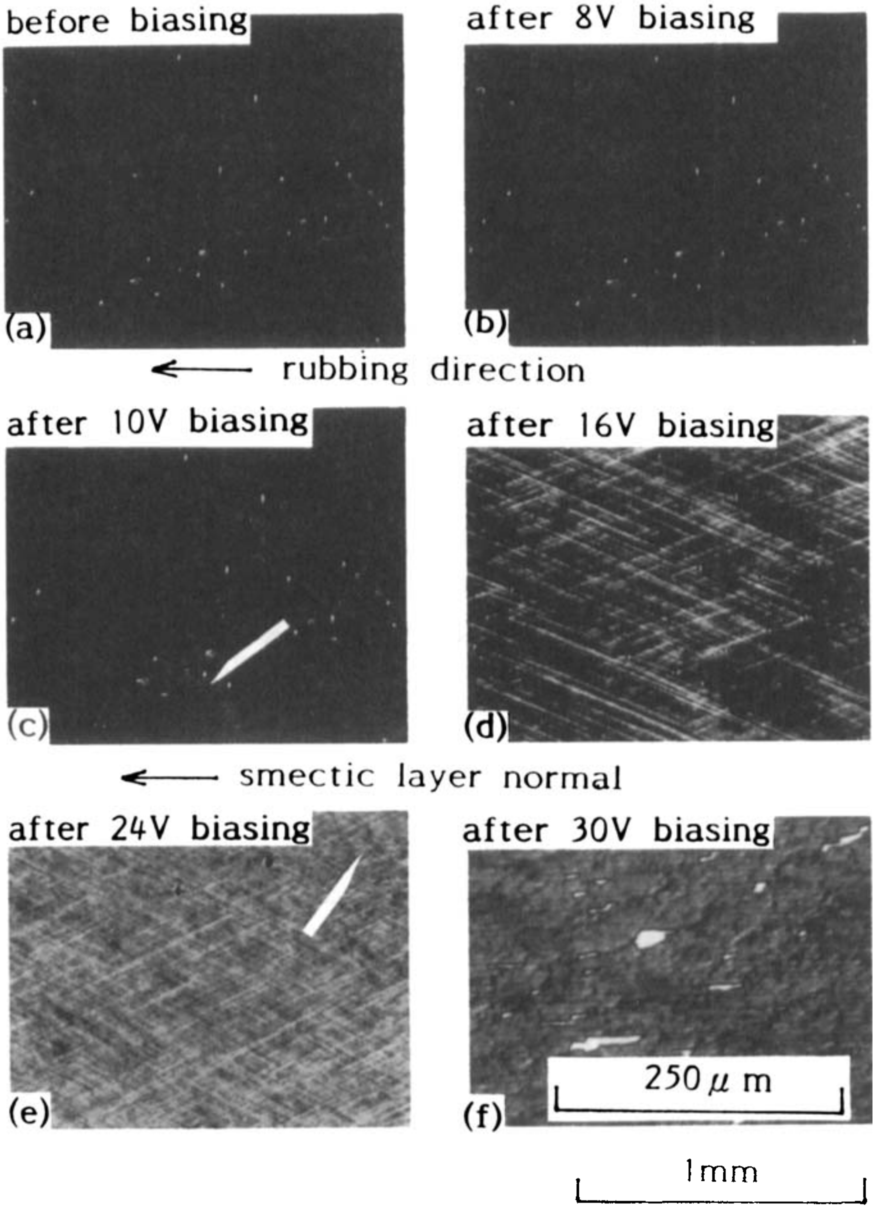

FIGURE 25 The polarized micrographs showing the textures of cell A: (a) before biasing, (b) after 8V biasing, (c) after 10V biasing, (d) after 16V biasing, (e) after 24V biasing and (f) after 30V biasing. See Color Plate XIV.

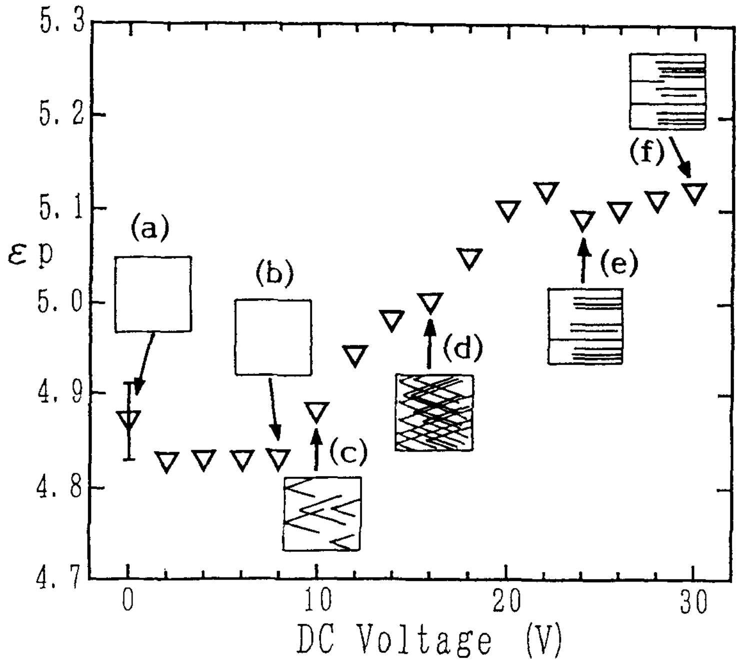

FIGURE 26 The voltage dependence of the dielectric permittivity of cell A at 10kHz after biasing.

and by texture observation. It was found that the smectic layer structure did not change below 8V biasing according to Figure 24 and Figure 26. The constant azimuthal angle Φ' when the appropriate voltage bias is applied, is determined from the voltage dependence of the apparent tilt angle $\theta_{app.}$, together with the simulation of the azimuthal angle dependence of the apparent tilt angle. Figure 20(c) shows the relationship between Φ' and $\theta_{app.}$. The apparent tilt angle $\theta_{app.}$ is expressed as

$$\theta_{app.} = \tan^{-1}\left(\frac{\sin\theta\cos\Phi'}{\sin\theta\sin\Phi'\sin\delta + \cos\theta\cos\delta}\right) \qquad (18)$$

The dielectric permittivity did not depend on the application time of the bias for low bias voltages below 8V, which was before the texture change. However the dielectric permittivity was dependent on the application time under high bias voltages over 10V because the texture change and the smectic layer deformation depend on the voltage, frequency and duration of the applied electric field. For the measurements at over 10V biasing, the final permittivity values during biasing are shown in Figure 23. Figure 27(a) shows the voltage dependence of the apparent tilt angles. Due to the texture changed after 10V measurement, the apparent tilt angles were measured for this changed texture. Figure 27(b) shows the simulated azimuthal angle dependence of the apparent tilt angles calculated by equation (18). The constant azimuthal angle Φ' was determined from Figure 27. Figure 27(b) was calculated for the half of the chevron layer structure in Figure 20(c) between the bottom surface and the chevron interface, and for the range of Φ' from $-\pi/2$(rad)[-90°] to $\pi/2$(rad)[90°]. It was assumed that Φ' lay between its initial value when no field was applied in Figure 11 and 0(rad) as shown in Figure 20(c). The apparent tilt angle $\theta_{app.}$ of cell A was 17.0° and that of cell B was 21.0°, both at 8V [Figure 27(a)]. The azimuthal angles Φ of the C2 state when the apparent tilt angle $\theta_{app.}$ is 17.0°, are -47.5° and 35.5°. Those of the C1 state when $\theta_{app.}$ is 21.0°, are -13.5° and 28°. See Figure 20(c) again. The constant azimuthal angle Φ' in the lower half of the chevron layer structure lies between 0(rad) and $\pi/2$(rad) for the C2 state, and between $-\pi/2$(rad) and 0(rad) for the C1 state, respectively. The constant azimuthal angle Φ' was determined to be 35.5° for cell A and -13.5° for cell B at 8V bias. The whole chevron layer structure was treated as symmetric about the chevron interface.

Novel Frequency Dependence of Dielectric Biaxiality

The three principal dielectric permittivities, calculated using the above procedure, are shown in Figure 28. These principal dielectric permittivities ε_1, ε_2 and ε_3 are almost equal for the two cells regardless of the different measured apparent permittivities. Two dielectric anisotropies, $\Delta\varepsilon$ and the dielectric biaxiality $\partial\varepsilon$, are shown in Figure 29. Both $\Delta\varepsilon$ and $\partial\varepsilon$ showed a similar slight frequency dependence. In particular $\partial\varepsilon$ showed an inversion around 1kHz. It was negative at 500Hz, almost zero at 1kHz, and then positive

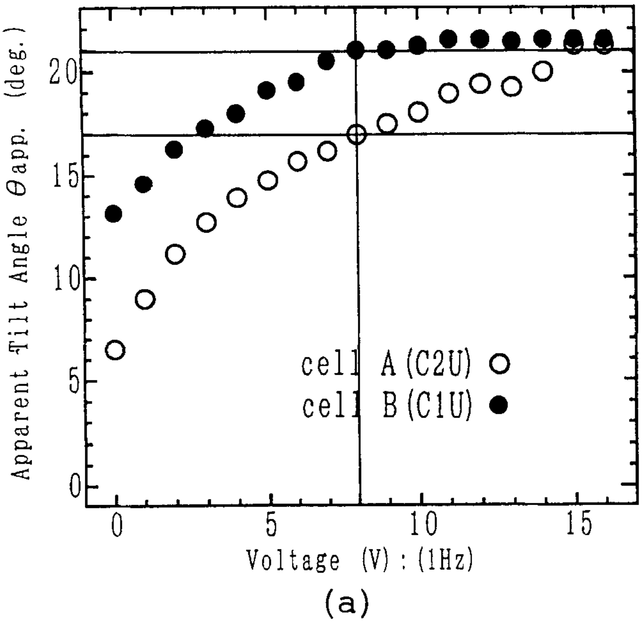

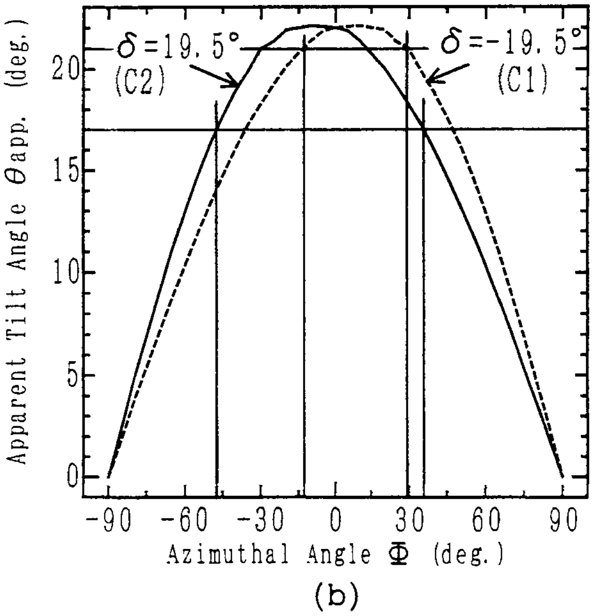

FIGURE 27 (a) The voltage dependences of the apparent tilt angles of the planar homogeneous cells. (b) The simulated azimuthal angle dependences of the apparent tilt angles. See text for explanation.

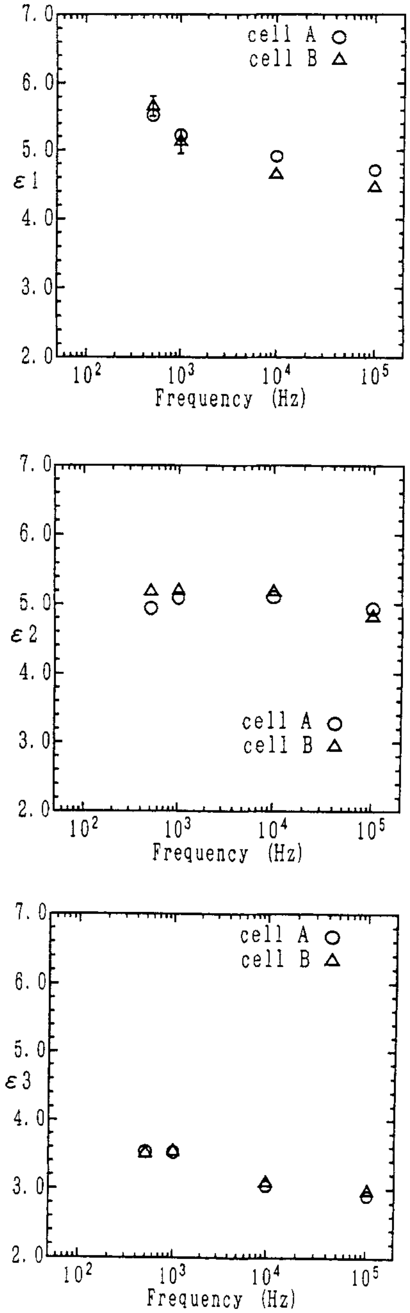

FIGURE 28 The frequency dependence of principal dielectric permittivities.

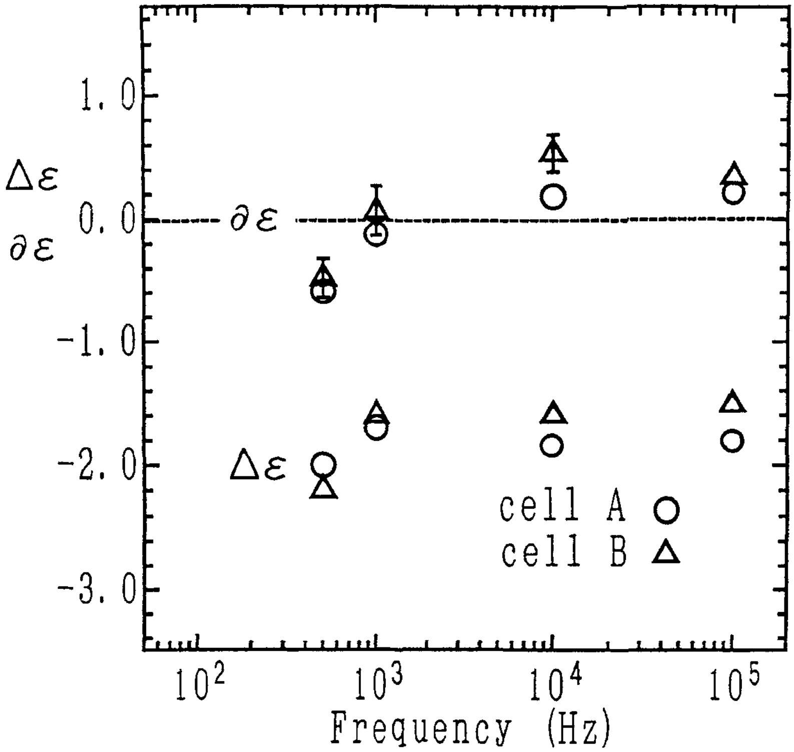

FIGURE 29 The frequency dependence of the two dielectric anisotropies, Δ ε and the dielectric biaxiality ∂ ε .

at 10kHz and 100kHz. The different frequency dependences of both the apparent dielectric permittivities during biasing in Figure 23 and after biasing in Figure 24 are explained by this novel frequency dependence of the dielectric biaxiality. The movement of the FLC molecule on the smectic cone is illustrated in Figure 30. The component of ε_2 in the dielectric permittivity of the SSFLC cell is increased by the bias field due to the rotation of the spontaneous polarization **p** towards to electric field [Figures 30(a) and 30(b)]. The smectic layer deformation from the chevron to the quasi-bookshelf structure also increases the component of ε_2 [Figures 30(a) and 30(c)]. Figure 30(d) shows the SSFLC structure during biasing after the smectic layer deformation. As reported in previous reports,[32,33] the smectic layer deformation progresses with increasing electric field treatment voltage. In this study it is the bias voltage which can cause the smectic layer deformation. With increasing the bias voltage, both the dielectric permittivities during biasing and after biasing increase if $\partial \varepsilon$ is positive, decrease if $\partial \varepsilon$ is negative and do not change if $\partial \varepsilon$ is zero. Therefore it is found that the movement of the FLC molecule on the smectic cone is strongly dominated by the dielectric biaxiality $\partial \varepsilon$.

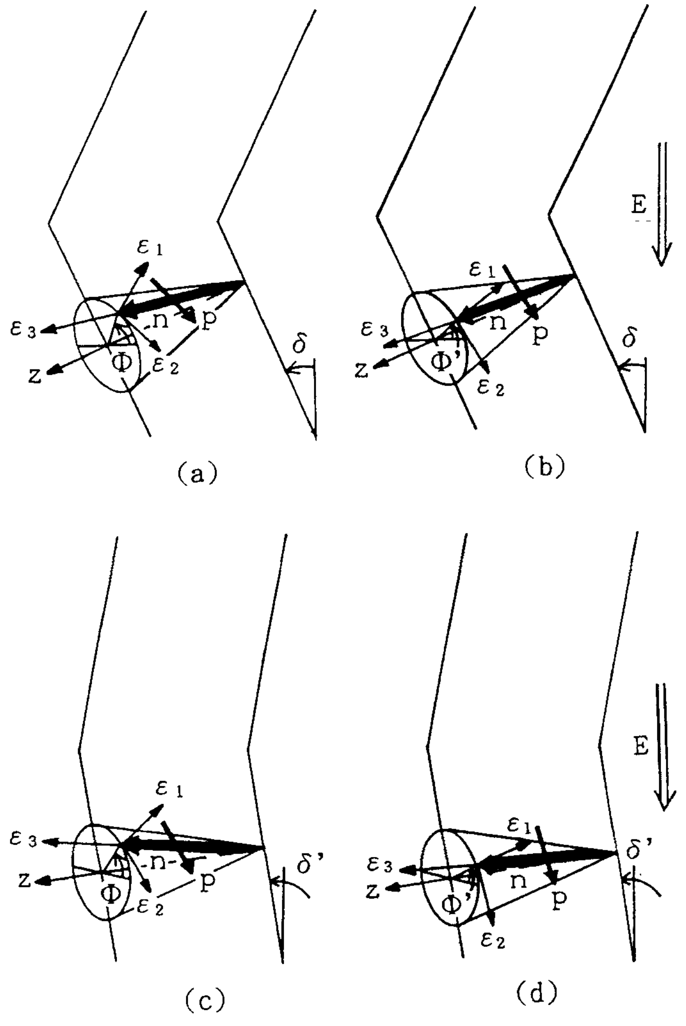

FIGURE 30 The movement of the FLC molecule on the smectic cone during biasing and after biasing. See text for explanation.

SUMMARY

The optical properties of SSFLCs is strongly dominated by the molecular orientational state. The technique of preparing a suitable state is one of major subjects not only for practical applications, but also to enable reliable experiments. An understanding for the effect of the surface pretilt angle is given by our molecular orientational models. However, it is found that differences between the theoretical and experimental results are remarkable in low pretilt regions of Figure 15. The behavior of FLC molecules near the surface, including the pretilt, is more complicated than for nematics. Research to elucidate this problem is the key study to make clear the mechanism of stability of the molecular orientational state and is now in progress.

Let us return to Figure 28 in order to discuss the novel behavior of the dielectric biaxiality with frequency. The dielectric permittivity ε_1 shows an obvious frequency dispersion, while ε_2 and ε_3 only slightly depend on the frequency. The theoretical explanation of these different frequency dependences of three dielectric permittivities are an interesting topics for a following.

ACKNOWLEDGMENTS

The authors thank Prof. E. P. Raynes and Dr. P. A. Gass of Sharp Laboratories of Europe Ltd. for helpful discussions and suggestions.

REFERENCES

1. N. A. Clark and S. T. Lagerwall, Appl. Phys. Lett., 36, 899 (1980).
2. N. Itoh, Y. Narutaki, T. Shinomiya, M. Koden, S. Miyoshi and T. Wada, Jpn. J. Appl. Phys., 31, 1414 (1992).
3. Y. Takanishi, Y. Ouchi, H. Takezoe, A. Fukuda, A. Mochizuki and M. Nakatsuka, Jpn. J. Appl. Phys., 29, L984 (1990).
4. T. P. Rieker, N. A. Clark, G. S. Smith, D. S. Parmar, E. B. Sirota and C. R. Safinya, Phys. Rev. Lett., 59, 2658 (1987).

5. Y. Ouchi, J. Lee, H. Takezoe, A. Fukuda, K. Kondo, T. Kitamura and A. Mukoh, Jpn. J. Appl. Phys., 27, L725 (1988).
6. N. A. Clark, T. P. Rieker and J. E. Maclennan, Ferroelectrics, 85, 79 (1988).
7. J. W. Goodby and E. Chin, J. Am. Chem. Soc., 108, 4736 (1986).
8. E. N. Keller, E. Nachaliel and D. Davidov, Phys. Rev. A, 34, 4363 (1986).
9. K. Suzuki, K. Toriyama and A. Fukuhara, Appl. Phys. Lett., 33, 561 (1978).
10. N. Itoh, M. Koden, S. Miyoshi and T. Wada, Liquid Crystals, 15, 669 (1993).
11. M. A. Handschy, N. A. Clark and S. T. Lagerwall, Phys. Rev. Lett., 51, 471 (1983).
12. Y. Ouchi, H. Takezoe and A. Fukuda, Jpn. J. Appl. Phys., 26, 1 (1987).
13. J. Kanbe, H. Inoue, A. Mizutome, Y. Hanyuu, K. Katagiri and S. Yoshihara, Ferroelectrics, 114, 3 (1991).
14. Y. Ouchi, H. Takano, H. Takezoe and A. Fukuda, Jpn. J. Appl. Phys., 27, 1 (1988).
15. N. A. Clark and T. P. Rieker, Phys. Rev. A., 37, 1053 (1988).
16. K. Okano and S. Kobayashi, Ekisyo Oyohen[in Japanese](Application of Liquid Crystals), 1985, (Baihukan Press), Chap. 2.
17. M. Koden, H. Katsuse, A. Tagawa, K. Tamai, N. Itoh, S. Miyoshi and T. Wada, Jpn. J. Appl. Phys., 31, 3632 (1992).
18. A. Tagawa, H. Katsuse, K. Tamai, N. Itoh, M. Koden, S. Miyoshi and T. Wada, Proc. Japan Display '92, Hiroshima, 1992, p519. (The Institute of Television Engineers of Japan, Tokyo, 1992).
19. J. E. Maclennan, N. A. Clark, M. A. Handschy and M. R. Meadows, Liquid Crystals, 7, 753 (1990).
20. S. J. Elston and J. R. Sambles, Jpn. J. Appl. Phys., 29, L641 (1990).
21. D. W. Berreman, J. Opt. Soc. Am., 62, 502 (1972).
22. M. Nakagawa and T. Akahane, J. Phys. Soc. Jpn., 55, 1516 (1986).
23. M. Kawaida, T. Yamaguchi and T. Akahane, Jpn. J. Appl. Phys., 28, L1602 (1989).
24. N. Itoh, M. Koden, S. Miyoshi, T. Wada and T. Akahane, Ferroelectrics, 147, 327 (1993).
25. N. Itoh, M. Koden, S. Miyoshi and T. Akahane, Liquid Crystals, in press.
26. P. W. H. Surguy, P. J. Ayliffe, M. J. Birch, M. F. Bone, I. Coulson, W. A. Crossland, J. R. Hughes, P. W. Ross, F. C. Saunders and M. J. Towler, Ferroelectrics, 122, 63 (1991).
27. J. R. Hughes and E. P. Raynes, Liquid Crystals, 13, 597 (1993).
28. M. Koden, H. Katsuse, N. Itoh, T. Kaneko, K. Tamai, H. Takeda, M. Shiomi, T. Numao, M. Kido, M. Matsuki, S. Miyoshi and T. Wada, Ferroelectrics, 149, 183 (1993).
29. J. C. Jones, M. J. Towler and E. P. Raynes, Ferroelectrics, 121, 91 (1991).
30. M. J. Towler, J. C. Jones and E. P. Raynes, Liquid Crystals, 11, 365 (1992).

31. N. Itoh, M. Koden, S. Miyoshi, T. Wada and T. Akahane, Jpn. J. Appl. Phys., 33, L241 (1994).
32. Y. Sato, T. Tanaka, H. Kobayashi, K. Aoki, H. Watanabe, H. Takeshita, Y. Ouchi, H. Takezoe and A. Fukuda, Jpn. J. Appl. Phys., 28, L483 (1989).
33. M. Isogai, M. Oh-e, T. Kitamura and A. Mukoh, Mol. Cryst. Liq. Cryst., 207, 87 (1991).